Electronic Supplementary Material (ESI) for

Facet-Dependent Solar Ammonia Synthesis of BiOCl Nanosheets via a Proton-Assisted Electron Transfer Pathway

Hao Li, Jian Shang, Jingu Shi, Kun Zhao, and Lizhi Zhang*

*Correspondence to: zhanglz@mail.ccnu.edu.cn

1. Materials and Methods

1.1 Preparation of BiOCl and SiO_2-coated BiOCl electrodes

To prepare BiOCl photoelectrodes, the photocatalysts were dispersed in chitosan solution to form a 10 $mg \cdot mL^{-1}$ solution. Then, 0.3 mL of colloidal solution was dip-coated on the pretreated FTO surface and was allowed to dry under vacuum conditions for 24 h at room temperature.

To prepare SiO_2 coated BiOCl, the above BiOCl electrodes were put in 40 mL ethanol and 10 mL H_2O at 40 ^oC for 30 min. Then 1.5 mL of NH_4OH (25 wt %) was added to the above dispersion. Then 0.05 mL of tetraethyl orthosilicate was quickly injected and the reaction continued for 2 h. The resultant electrodes (denoted as BOC-001-SiO_2 or BOC-010-SiO_2) were washed with water and absolute ethanol, and finally dried under vacuum conditions for 24 h at room temperature.

1.2 Materials characterization

The powder X-ray diffraction (XRD) were recorded on a Rigaku D/MAX-RB diffractometer with monochromatized Cu Kα radiation (λ = 0.15418 nm). The scanning electron microscope (SEM) images and energy-dispersive X-ray spectrum (EDS) were obtained with a JEOL 6700-F field-

emission scanning electron microscope. The transmission electron microscopy (HRTEM) images were obtained by JEOL JSM-2010 high-resolution transmission electron microscopy. UV-visible absorbance spectra of the samples were obtained using a UV-visible spectrophotometer (UV-2550, Shimadzu, Japan). Electron paramagnetic resonance (EPR) spectra were conducted on a Bruker EMX EPR Spectrometer (Billerica, MA). N_2 temperature-programmed desorption experiments (N_2-TPD) were performed in a quartz reactor using a TCD as detector. 0.3 g catalyst was first pre-treated with pure He with a flow rate of 50 ml min^{-1} at 120 °C for 30 min, then cooled down to room temperature in the same atmosphere and then dosed with pure N_2. The catalyst was then purged with pure He (99.999%) gas with a flow rate of 50 ml min^{-1} for 30 min to remove the residual N_2. Then, the N_2-TPD measurement was performed up to 400 °C at a heating rate of 5 °C min^{-1} in the pure He atmosphere. *In situ* diffuse reflectance FTIR spectra were recorded by Nicolet iS50FT-IR spectrometer (Thermo, USA).

2. Supplementary figures and text

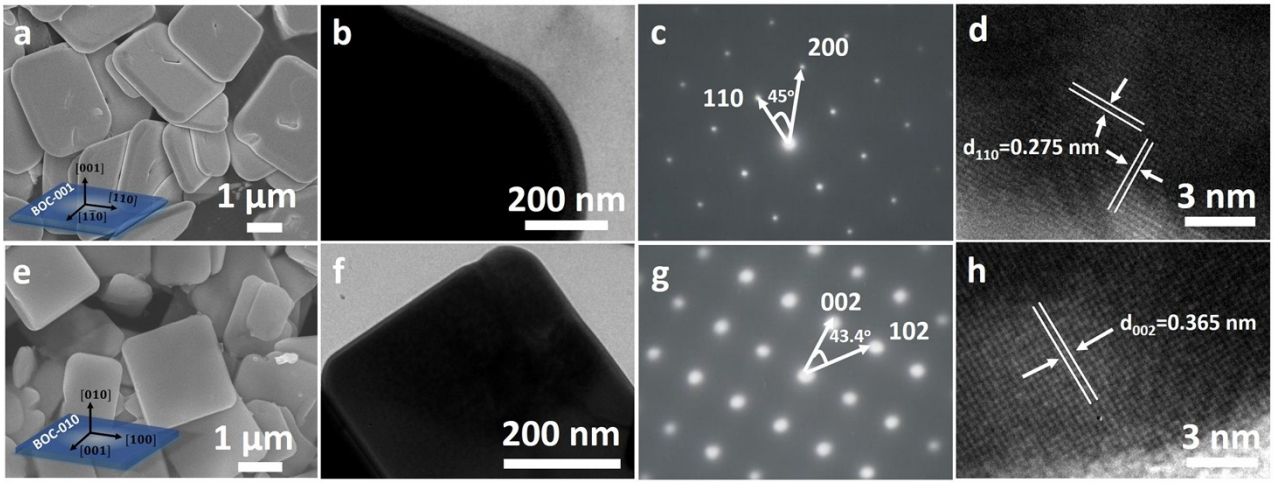

Figure S1. (a) SEM image, (b) TEM image, (c) corresponding SAED pattern and (d) HRTEM image of the BOC-001 nanosheets. (e) SEM image, (f) TEM image, (g) corresponding SAED pattern and (h) HRTM image of the BOC-010 nanosheets.

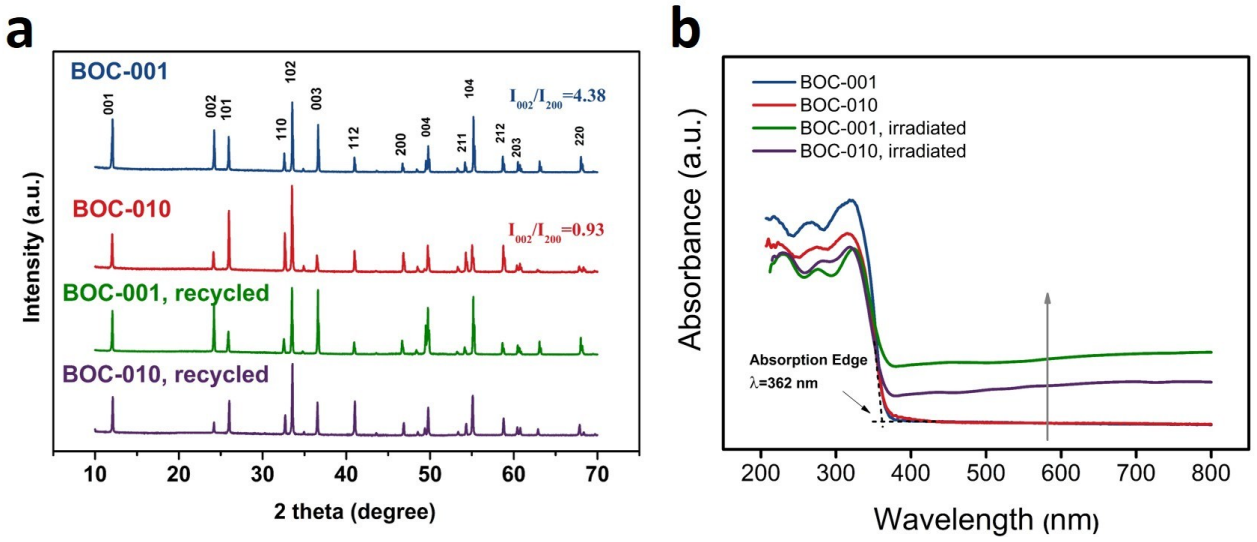

Figure S2. (a) XRD pattern of the as-prepared and recycled BiOCl. (b) UV-vis absorbance spectra of the as-prepared and solar-light-irradiated BiOCl.

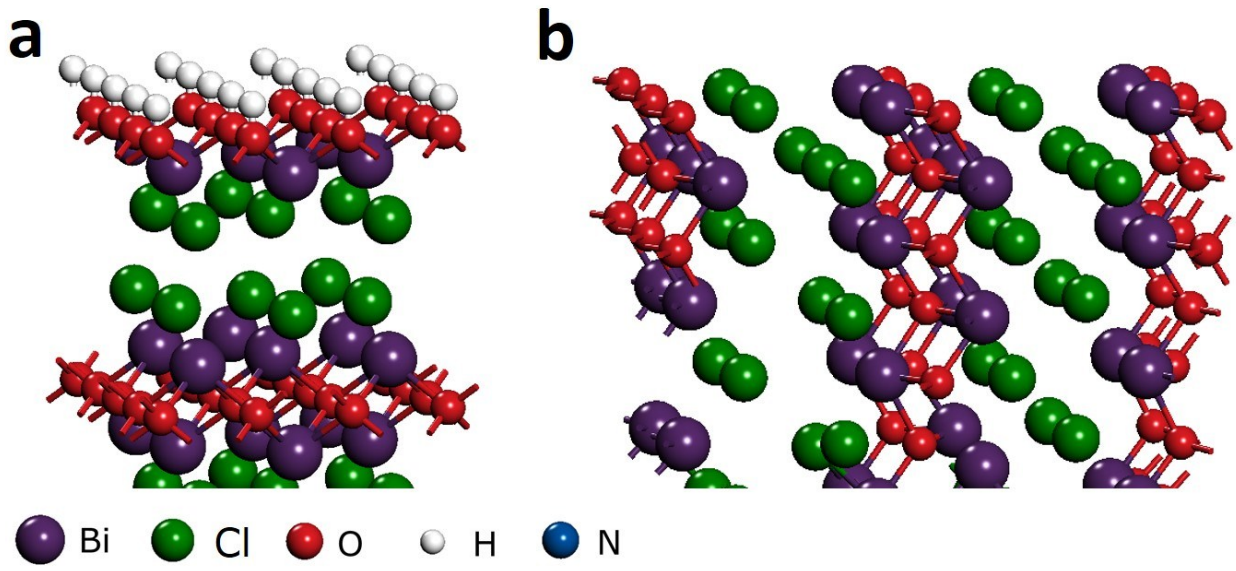

Figure S3. Structure of simulated (a) BiOCl (001) surface and (b) (010) surface.

Characterization of BOC-001 and BOC-010 single-crystalline nanosheets: SEM images revealed that BOC-001 consisted of large-scale decahedron-shaped single crystalline nanosheets with widths of 4~8 μm and thickness of 400~500 nm (Figure S1a). The percentage of {001} facets was estimated to be 71%. The TEM diffraction spots and corresponding SAED of BOC-001 nanosheet were indexed as the [001] zone of tetragonal BiOCl and the displayed (110) and (200) planes with an angle of 45° was in agreement to the theoretical value (Figure S1b and S1c). The lattice fringe spacing of 0.73 nm on the HRTEM image of vertical nanosheet was assigned to the (001) planes of BOC-001 (Figure S1d).

The BOC-010 consisted of sheet-shaped single crystalline nanosheets with width of 1~3μm and thickness of 100~300 nm (Figure S1e). The percentage of {010} facets was estimated to be 77%. The corresponding SAED pattern was indexed as [010] zone. The displayed (002) and (102) planes with an angle of 43.4° was close to the theoretical value (Figure S1f and S1g). The (002) atomic

plane with a lattice spacing of 0.37 revealed that the BOC-010 nanosheets were exposed with {010} facets (Figure S1h).

X-ray diffraction (XRD) characterization showed that the intensity ratios of (002) and (200) peaks were respectively 4.38 and 0.93 for BOC-001 and BOC-010, which indirectly reflected the different facet exposure of these two samples (Figure S2a). Both BiOCl exhibited a defect-free absorption edge 362 nm in the UV region and no absorption in the visible-light region (Figure S2b).

Figure S3 shows the simulated (001) and (010) surface structures of BiOCl, in which (001) surface exhibits a close-packed structure with O atom exposed and (010) surface exhibits an open structure with both O, Bi and Cl exposed. The addition of a layer H atoms is used to stabilize the {001} surface, considering the abundant protons in acid solution (pH = 1) during the synthesis of BOC- 001 and the strong H−O bonding energy of 428 kJ/mol.[1-3] For simplicity, such layer of H atoms are not shown in the manuscript.

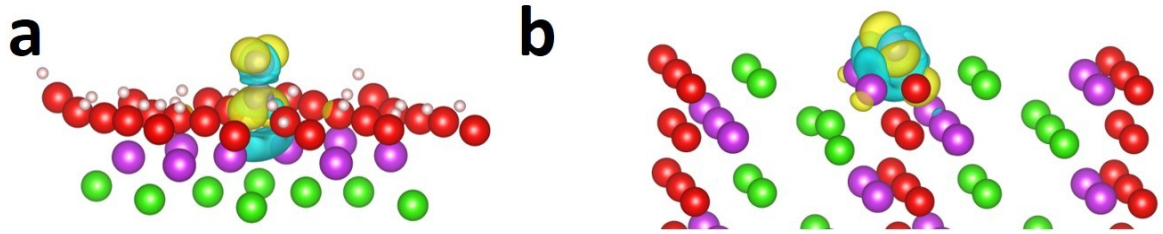

Figure S4. The charge density difference of the N_2 adsorbed (a) BOC-001 and (b) BOC-010. The yellow and blue isosurfaces represent charge accumulation and depletion in the space, respectively. The isovalue was 0.002 au.

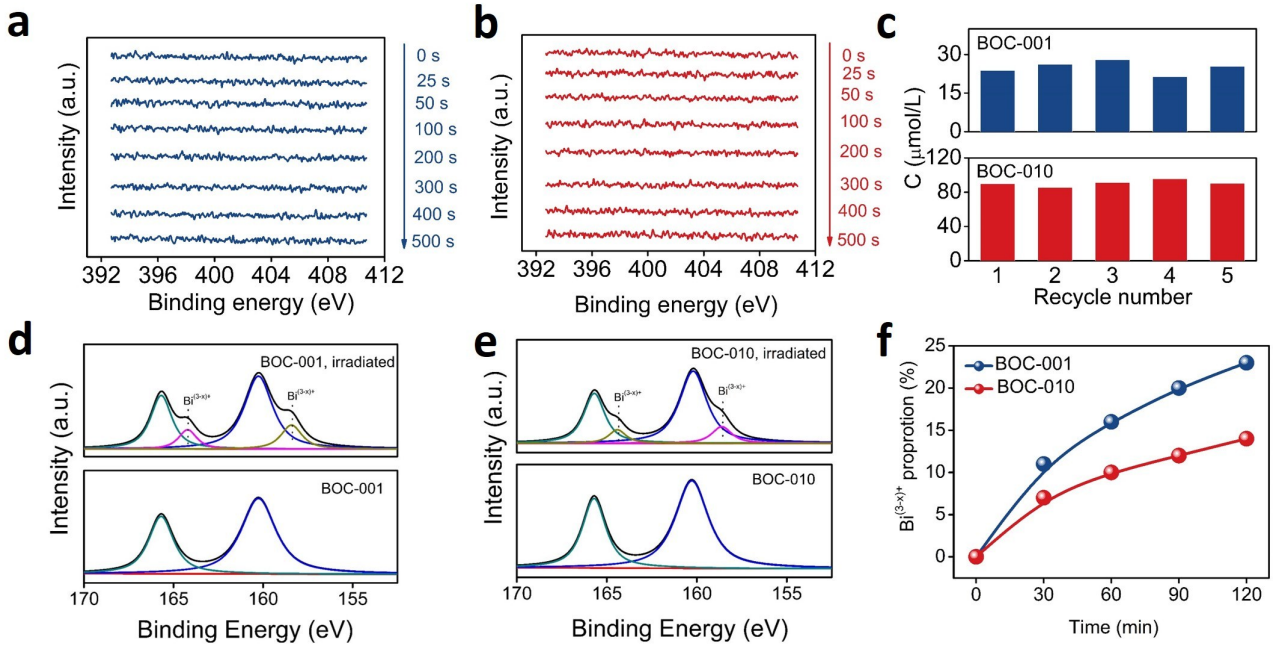

Figure S5. Time-dependent high resolution N 1s XPS spectra of (a) BOC-001 and (b) BOC-010 upon Ar^+. (c) NH_3 generation over the as-prepared BiOCl for repeated use. High-resolution Bi 4f XPS spectra of (d) BOC-001 and (e) BOC-010. (f) Proportion of low-valent $Bi^{(3-x)+}$ of the as-prepared BiOCl under solar light along with time.

Figure S5d and 5e shows the high-resolution Bi 4f XPS of the as-prepared BiOCl before and after irradiation under solar light for 2 h. Both BOC-001 and BOC-010 exhibited two additional peaks of lower binding energy ascribed to the partial reduction of Bi^{3+} via localized electrons on OVs. The concentrations of OVs could be indirectly reflected by the proportion of $Bi^{(3-x)+}$ peak areas, which was respectively 23% for BOC-001 and 15% for BOC-010. Therefore, BOC-001 was more inclined to form OVs than BOC-010. Theoretically, the (001) surface of BiOCl requires 2.8 eV of energy less than the (010) surface to form an OV. We further monitored the concentration variation of OVs according to the time-dependent change of low-valent $Bi^{(3-x)+}$ proportion under solar light, and found the OVs generation rate of BOC-001 was much faster than that of BOC-010 (Figure S5f). Besides,

the higher absorption tail intensity in BOC-010 indicates more OVs were formed on the {001} facets than those on the {010} facets after solar light irradiation, which was consistent with the above XPS analysis (Figure S2b).

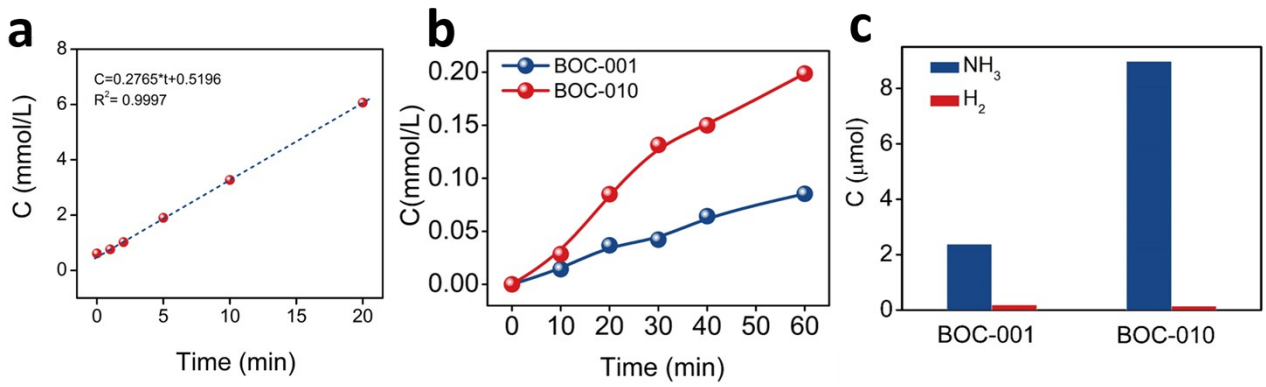

Figure S6. (a) The concentration of generated Fe^{2+} during the photoreduction of potassium ferrioxalate. (b) Quantitative determination of the generated NH_3 over BiOCl under the UV light. (c) Generated H_2 in comparison with the NH_3 over the as-prepared BiOCl.

A UV light (λ = 254 nm) lamp was used to determine the quantum yields of BOC-001 and BOC-010. The apparent quantum yield is generally calculated based on the following equation: apparent quantum yield = [number of reacted electrons]/[number of incident photons]. The number of reacted electrons are determined from the amount of detected NH_3 and the number of incident photons reaching the reacting space can be indirectly determined by a chemical actinometry using potassium ferrioxalate considering that quantum yield of the potassium ferrioxalate at 254 nm is 1.25.[4-6] The rate of potassium ferrioxalate photolysis under UV light in our system was estimated to be 0.2765 $mmol \cdot L^{-1} \cdot min^{-1}$ (Figure S6a). According to the detected NH_3 concentration under UV light, the apparent quantum yields were estimated to be 1.8% for BOC-001 and 4.3% for BOC-010 within 60 min, respectively (Figure S6b).

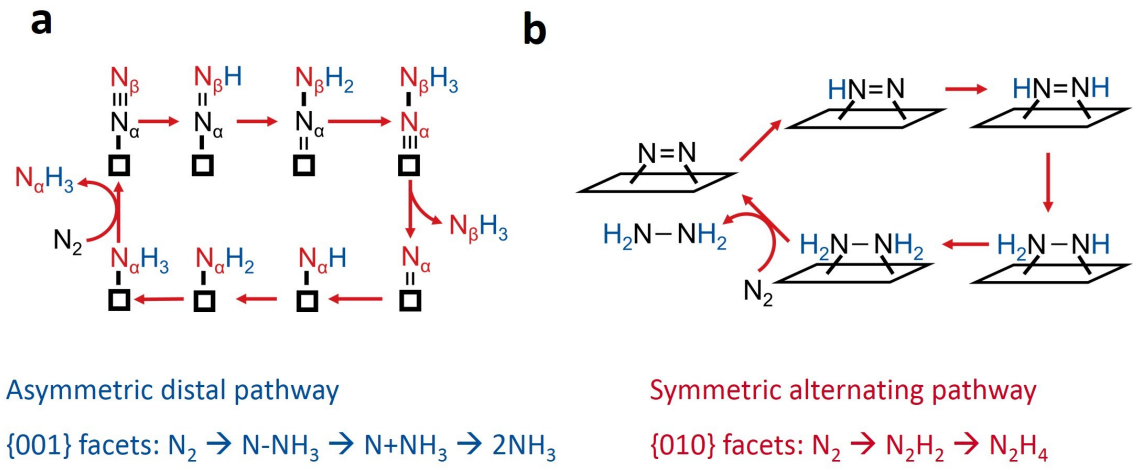

Figure S7. Schematic illustration of the N_2 fixation scheme following the (a) distal pathway of terminal end-on bound N_2 and (b) alternating pathway of side-on bridging bound N_2.

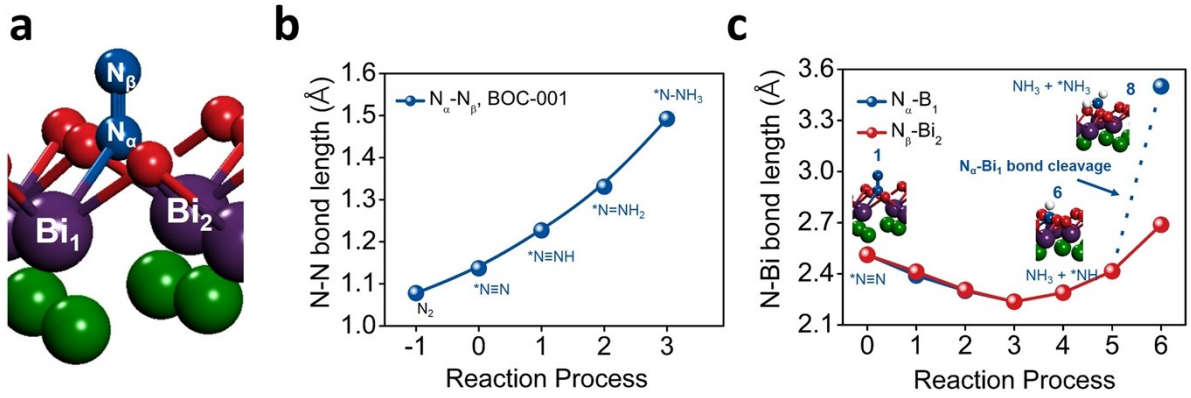

Figure S8. (a) Structure of N_2 adsorbed BOC-001 surface. Dynamic change of (b) the N-N bond order and (c) N-Bi bond length during the N_2 fixation process on the (001) surface.

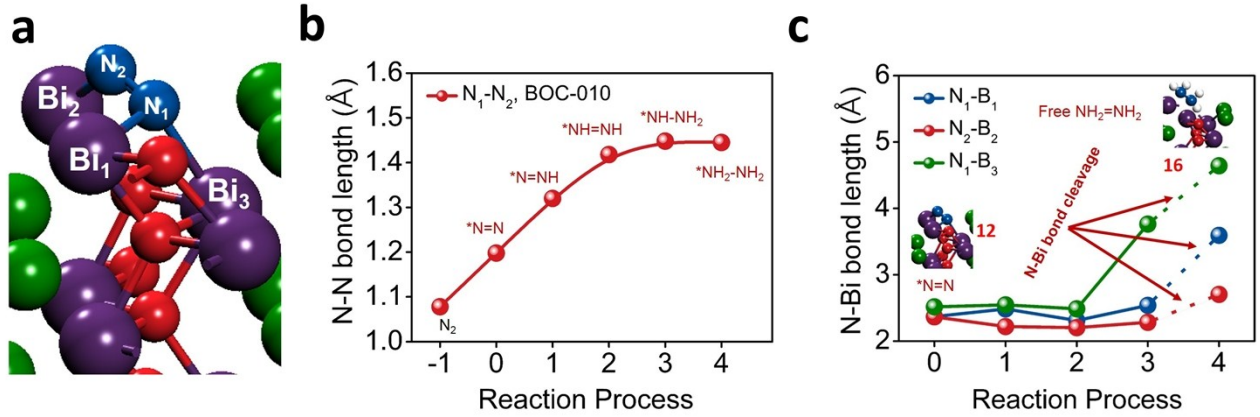

Figure S9. (a) Structure of N_2 adsorbed BOC-010 surface. Dynamic change of (b) the N-N bond order and (c) N-Bi bond length during the N_2 fixation process on the (010) surface.

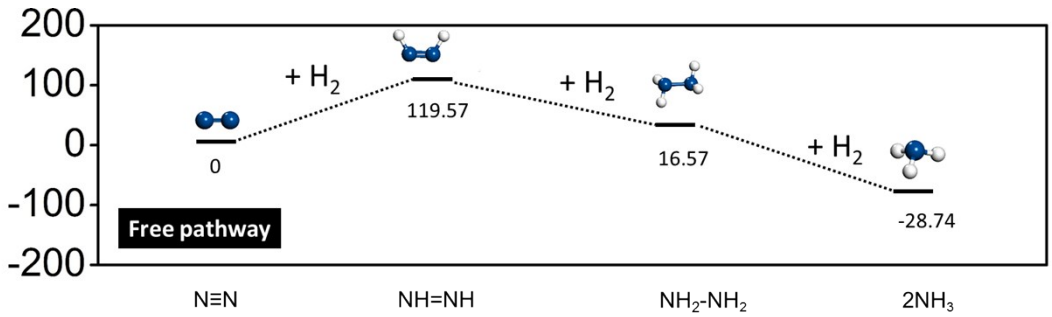

Figure S10. Free (uncatalyzed) N_2 fixation pathway using H_2 as the proton source and electron carrier.

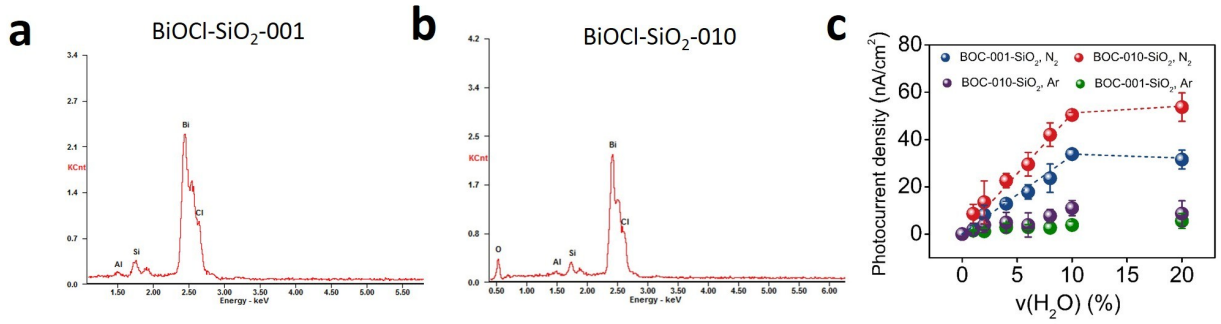

Figure S11. EDS spectra of the as-prepared SiO_2 coated (a) BOC-001 and (b) BOC-010 electrode. (c) The photocurrent density (PE3) reflecting the electron transfer from BiOCl to N_2 as a function of the proportion of water in CH_3CN. The Ar purging was used for comparison. The error bars arise from values extracted from several measurements on multiple catalysts.

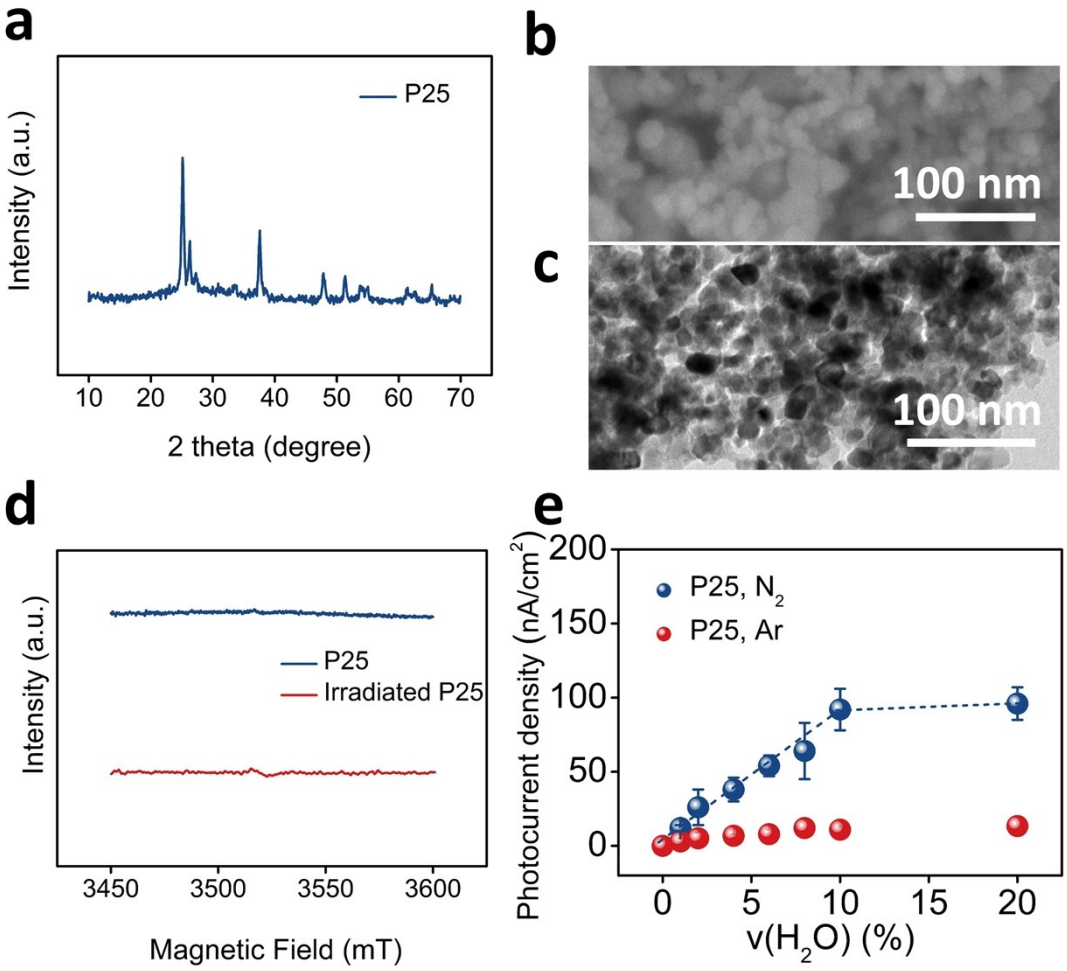

Figure S12. (a) XRD pattern, (b) SEM, (c) TEM images and (d) EPR spectra of TiO_2-P25. (e) The photocurrent density (PE3) reflecting the electron transfer from BiOCl to N_2 as a function of the proportion of water in CH_3CN. The Ar purging was used for comparison. The error bars arise from values extracted from several measurements on multiple catalysts.

Figure S12a-c are respectively the XRD pattern, SEM and TEM image of TiO_2-P25. According to the EPR spectra, different from BiOCl, the P25 exhibited no significant signal of OV after being irradiated by solar light for 2 h (Figure S12d).

Table S1. Bader charges (Q (e)) of Bi atoms neighboring to OV and adsorbed N_2 ($(N_2)_{ad}$) in the slabs

	BOC-001	**BOC-001 + OV**	**BOC-001 + OV-N_2**
Bi_1, Bi_2	2.85	3.47	2.96
$(N_2)_{ad}$	-	-	10.41
	BOC-010	**BOC-010 + OV**	**BOC-010 + OV-N_2**
Bi_1	3.13	3.87	3.35
Bi_2	3.13	3.95	3.23
Bi_3	3.04	3.07	3.12
$(N_2)_{ad}$	-	-	11.15

Bader charge analysis: According to the Bader charge, after generation of an OV on the (001) surface, the electrons are mainly localized on the two nearest Bi atoms and are transferred to the adsorbed N_2 after its adsorption (Table S1). Similarly, the localized electrons after the generation of an OV on the (010) surface are mainly gathered at the Bi_1, Bi_3 and Bi_3 atoms. The transfer of these localized electrons on the OV of (010) facet to the adsorbed N_2 is also obvious after the N_2 adsorption. Notably, more electrons are transferred to N_2 adsorbed on the OV of (010) surface (11.15 e), which explains its larger N_2 activation extent

Table S2. Physical properties and photocatalytic activity of the samples

Sample	A_{BET} ($m^2 g^{-1}$)	k_{NH3} ($\mu mol\ h^{-1}$)	k'_{NH3} ($\mu mol\ g\ h^{-1}\ m^{-2}$)	k_{N2H4} ($\mu mol\ h^{-1}$)	k'_{N2H4} ($\mu mol\ g\ h^{-1}\ m^{-2}$)
BOC-001	0.63	1.19	**1.89**	-	-
BOC-010	2.01	1.92 (0-0.5 h)	**0.95**	8.33 (0-0.5 h)	4.14
		4.62 (0.5-2 h)	**2.29**		
TiO_2-P25	42.53	3.79 (0-2 h)	**0.09**	-	-

[a] The *k*' values were *k* values normalized with the surface areas.

Table S3. Calculated energy and zero point energy of the corresponding free and adsorbed molecules.

Structure	Energy (kcal/mol)	Zero point energy Energy (kcal/mol)	Corrected energy Energy (kcal/mol)
BOC-001-N_2	-15505.09	4.39	-15500.70
BOC-001-N_2H	-15553.59	11.17	-15542.42
BOC-001-N_2H_2	-15606.77	19.11	-15587.66
BOC-001-N_2H_3	-15672.25	26.88	-15645.37
BOC-001-N_2H_4	-15749.10	29.09	-15720.01
BOC-001-N_2H_5	-15860.12	37.77	-15822.35

BOC-001-N_2H_6	-15892.67	45.15	-15847.52
BOC-010-N_2	-9262.12	4.71	-9257.41
BOC-010-N_2H	-9321.89	11.23	-9310.66
BOC-010-N_2H_2	-9404.75	18.41	-9386.34
BOC-010-N_2H_3	-9520.94	26.20	-9494.74
BOC-010-N_2H_4	-9519.82	33.85	-9485.97
NH_3	-449.37	21.19	-428.17
N_2H_2	-430.15	21.10	-409.05
N_2	-382.58	3.46	-379.13
N_2H_4	-693.88	32.34	-661.54
H_2	-155.75	6.26	-149.49

References:

1. K. Zhao, L. Z. Zhang, J. J. Wang, Q. X. Li, W. W. He and J. J. Yin, *J. Am. Chem.*, *Soc.*, 2013, **135**, 15750.
2. H. G. Yang, C. H. Sun, S. Z. Qiao, J. Zou, G. Liu, S. C. Smith, H. M. Cheng and G. Q. Lu, *Nature*, 2008, **453**, 638.
3. J. A. Dean, Lange's Handbook of Chemistry, 15th ed.; McGraw-Hill: NewYork, 1998.
4. C. G. Hatchard, C. A. Parker, *Proc. R. Soc. London. Ser. A* 1956, **235**, 518.
5. Y. Quan , S. O. Pehkonen, M. B. Ray, *Ind. Eng. Chem. Res.* 2004, **43**, 948.
6. L. Sun, J. Bolton, *J. Phys. Chem. B*, 1996, **100**, 4127.